Int. J. Heat Mass Transfer. Vol. 10, pp. 951–965. Pergamon Press Ltd. 1967. Printed in Great Britain

FORCED CONVECTION SUBCOOLED BOILING—PREDICTION OF VAPOR VOLUMETRIC FRACTION

S. LEVY

General Electric Company, Atomic Power Equipment Department, San Jose, California

(*Received* 28 *July* 1966 *and in revised form* 8 *December* 1966)

Abstract—A model is developed to predict the vapor volumetric fraction during forced convection subcooled boiling. The proposed method of calculation consists of three steps:

1. The point of bubble departure from the heated surface (i.e. the location of vapor volumetric fractions significantly higher than zero) is determined from a bubble force balance and the single-phase liquid turbulent temperature distribution away from the heated wall.
2. A relation is postulated between the true local vapor weight fraction and the corresponding thermal equilibrium value.
3. The vapor volumetric fraction is obtained from the true local vapor weight fraction and an accepted relationship between vapor weight and volumetric fractions.

The method was applied to a variety of available test data, and the agreement was satisfactory for a multitude of flow, heat flux, and fluid property conditions.

NOMENCLATURE

A, heat-transfer area [ft^2];
A_F, flow area [ft^2];
C, C', C_B, C_S, C_F, constants;
C_p, specific heat [Btu/lb-°F];
D_H, hydraulic diameter [ft];
F, force [lb];
f, friction factor [nondimensional];
G, mass flow area per unit area [lb/h-ft^2];
g, gravitational constant [ft/h^2];
g_c, conversion from lb-force to lb-mass;
H_{fg}, heat of vaporization [Btu/lb];
h, heat-transfer coefficient [Btu/h-ft^2-°F];
N_{Pr}, Prandtl number [nondimensional];
P_W, wetted perimeter [ft];
p, pressure [lb/ft^2];
Q, nondimensional heat input given by equation (14);
q, local heat input [Btu/h];
r_B, vapor bubble radius;
S, spacing between vapor bubbles [ft];
T_B, temperature at tip of bubbles [°F];
T_S, saturation temperature [°F];
T_W, wall temperature [°F];
U_{rel}, relative bubble velocity [ft/h];
Y_B, distance from wall corresponding to tip of vapor bubble [ft];
Y_B^+, nondimensional distance to tip of vapor bubble;
z, distance along flow channel [ft].

Greek symbols

α, vapor volumetric fraction;
ΔT, saturation temperature minus local bulk fluid temperature [°F];
ϵ, channel roughness [ft];
χ, thermal equilibrium vapor weight fraction;

χ', true local vapor weight fraction;
μ, absolute viscosity [lb/h-ft];
ρ, density [lb/ft^3];
σ, surface tension [lb/ft];
τ_w, wall shear stress [lb/ft^2].

Subscripts

d, point of bubble departure from heated wall;
L, liquid;
V, vapor.

1. INTRODUCTION

ONE OF the most important nonthermal equilibrium two-phase flow processes is that of subcooled forced convection boiling. In such a system, heat is being added to a subcooled fluid as it flows past a heated surface and, as shown in Fig. 1, vapor bubbles and liquid below saturation can be found simultaneously at a given cross section. The boiling flow depicted in Fig. 1 can be broken down into four regions as suggested by Bowring [1]. To the left of point A, no vapor is present and normal forced convection cooling prevails. At point A, the first vapor bubble appears, and from A to B more and more bubbles are formed along the heater surface. In the region AB, the thickness of the superheated liquid layer close to the wall is small, and the bubbles cannot grow to a size large enough to leave the surface. At point B, the first bubble departs from the heated wall and the vapor volumetric fraction starts to rise sharply. From point B to C, even though the vapor volumetric fraction is large, nonthermal equilibrium conditions exist; in other words, some of the flowing liquid is still subcooled and the local vapor weight fraction is higher than would be calculated from a heat balance. At the location C, all of the liquid is at saturation temperature and thermal equilibrium conditions have finally been established.

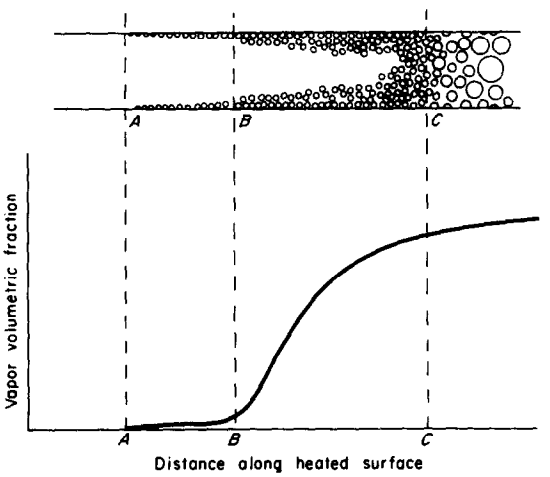

FIG. 1. Vapor volumetric fraction during forced convection subcooled boiling.

Because of its importance in liquid-cooled nuclear reactors, several attempts have been made to predict the shape of the curve shown in Fig. 1. Most of these efforts to-date have been empirical due to the complex nature of the subcooled boiling process. Early correlations were presented by Griffith, Clark, and Rohsenow [2] and by Maurer [3]. A more comprehensive approach was next offered by Bowring [1], who developed empirical expressions for the point where the vapor bubbles first leave the heated surface and for the fraction of heat which goes to form vapor bubbles. More recently, Zuber, Staub, and Bijwaard [4] postulated a profile for the liquid temperature during nonthermal equilibrium conditions, and derived an expression for the vapor volumetric fraction which takes into account the vapor concentration profile across the flow duct and the local relative velocity between the two phases. One of the important shortcomings of the preceding analysis is that it does not prescribe a method for calculating the location of point B in Fig. 1. It is the purpose of this report to obtain an expression which determines the position where vapor bubbles first leave the heated surface. A relation similar to that presented in [4] is next postulated for the vapor weight fraction, and the corresponding vapor volumetric fraction can be predicted and compared to available test data.

2. PREDICTION OF POINT OF DEPARTURE OF VAPOR BUBBLES FROM HEATED SURFACE

The position where vapor bubbles first leave the heated surface is obtained from two considerations:

1. A balancing of the forces exerted on the vapor bubble while it is in contact with the wall, and
2. The temperature distribution in the single-phase liquid away from the wall.

The forces acting on the bubble in the flow direction are shown in Fig. 2 for the case of

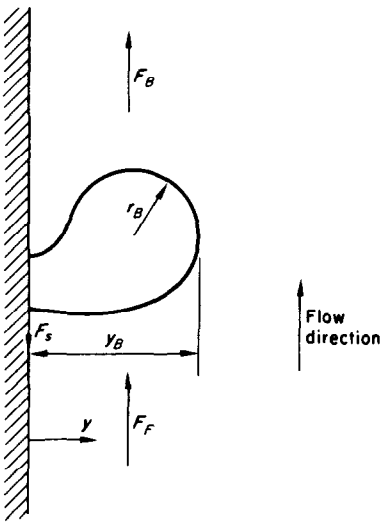

FIG. 2. Vapor bubble prior to departure from heated surface.

vertical upwards flow. They consist of a buoyant force, F_B; a vertical component, F_S of the surface tension force; and a frictional force, F_F, exerted by the liquid upon the bubble. The buoyant force, F_B, is given by

$$F_B = \frac{C_B r_B^3 (\rho_L - \rho_V) g}{g_c} \tag{1}$$

where r_B is the bubble radius, C_B is a proportionality constant, ρ_L and ρ_V are the liquid and vapor density, g is the gravitational constant, and g_c is a conversion ratio from lb-force to lb-mass. Similarly, the surface tension force, F_S, can be expressed as follows:

$$F_S = C_S r_B \sigma, \tag{2}$$

where C_S is a proportionality constant, and σ is the surface tension. Finally, the force F_F can be related to the liquid frictional pressure drop per unit length, $(-\mathrm{d}p/\mathrm{d}z)_F$. The pressure differential seen by the bubble is proportional to $(-\mathrm{d}p/\mathrm{d}z)_F$ r_B, and it acts across an area proportional to r_B^2. If we now relate the frictional pressure $(-\mathrm{d}p/\mathrm{d}z)_F$ to the wall shear stress τ_w according to

$$\left(-\frac{\mathrm{d}p}{\mathrm{d}z}\right)_F = \frac{4\tau_w}{D_H}, \tag{3}$$

there results for F_F

$$F_F = C_F \frac{\tau_w}{D_H} r_B^3, \tag{4}$$

where C_F is a proportionality constant, and D_H is the hydraulic diameter taken equal to four times the cross-sectional area divided by the wetted perimeter. A force balance applied to the bubble shown in Fig. 2 gives

$$C_B \frac{g}{g_c}(\rho_L - \rho_V) r_B^3 + C_F \frac{\tau_w}{D_H} r_B^3 - C_S r_B \sigma = 0. \tag{5}$$

Solving for the bubble radius, r_B yields

$$r_B = \sqrt{\left(\frac{C_S \sigma}{C_B \frac{g}{g_c}(\rho_L - \rho_V) + C_F \frac{\tau_w}{D_H}}\right)}. \tag{6}$$

We assume next that the distance Y_B to the tip of the bubble is proportional to r_B, and we can rewrite equation (6) as follows:

$$Y_B = C\left(\frac{\sigma D_H}{\tau_w}\right)^{\frac{1}{2}} \left[1 + C' \frac{g}{g_c} \frac{(\rho_L - \rho_V) D_H}{\tau_w}\right]^{-\frac{1}{2}} \tag{7}$$

Equation (7) specifies the distance Y_B to the tip of the bubble. The corresponding non-dimensional distance Y_B^+ is given by

$$Y_B^+ = Y_B\left(\sqrt{\frac{\tau_w g_c}{\rho_L}}\right)\frac{\rho_L}{\mu_L} = C \frac{(\sigma g_c D_H \rho_L)^{\frac{1}{2}}}{\mu_L} \left[1 + C' \frac{g}{g_c} \frac{(\rho_L - \rho_V) D_H}{\tau_w}\right]^{-\frac{1}{2}}. \tag{8}$$

For the case where the fluid forces acting on the bubble are much larger than the buoyant forces, equation (8) reduces simply to

$$Y_B^+ = C(\sigma g_c D_H \rho_L)^{\frac{1}{2}} \frac{1}{\mu_L}. \tag{9}$$

Let us next consider the temperature distribution within the liquid. As originally pointed out by Hsu [5], the fluid temperature T_B at position Y_B must exceed the saturation temperature by a prescribed amount such as

$$\Delta p = \frac{2\sigma}{r_B}, \tag{10}$$

where Δp is the pressure differential acting across the interface at the tip of the bubble to balance the surface tension forces at that same position. Substituting for Δp from the Clausius–Clapeyron relation gives

$$T_B - T_S = \frac{2\sigma T_S(\rho_L - \rho_V)}{\rho_V H_{fg} r_B \rho_L}, \tag{11}$$

where T_S is the saturation temperature, and H_{fg} is the heat of vaporization. For simplification purposes, it will be assumed that the right-hand side of equation (11) is close to zero* and

$$T_B = T_S. \tag{12}$$

The temperature T_B at the position Y_B^+ can also be specified from existing solutions for the fluid temperature distribution. If we assume that the flow is turbulent and if we utilize the solution proposed by Martinelli [6], there results

$$\left.\begin{aligned} T_w - T_B &= QN_{Pr}Y_B^+, && 0 \leqslant Y_B^+ \leqslant 5 \\ T_w - T_B &= 5Q\left\{N_{Pr} + \ln\left[1 + N_{Pr}\left(\frac{Y_B^+}{5} - 1\right)\right]\right\}, && 5 \leqslant Y_B^+ \leqslant 30 \\ T_w - T_B &= 5Q\left\{N_{Pr} + \ln\left[1 + 5N_{Pr}\right] + 0{\cdot}5\ln\left[\frac{Y_B^+}{30}\right]\right\}, && Y_B^+ > 30 \end{aligned}\right\} \tag{13}$$

where N_{Pr} is the liquid Prandtl number, and Q is a nondimensional term defined in terms of the local heat flux (q/A) and the liquid specific heat C_{pL}:

$$Q = \frac{q/A}{\rho_L C_{pL}\left(\sqrt{\frac{\tau_w g_c}{\rho_L}}\right)}. \tag{14}$$

By setting $T_B = T_S$ and introducing the definition of the heat-transfer coefficient h in terms of the liquid mixed mean temperature T_f,

$$T_w - T_f = \frac{q/A}{h} \tag{15}$$

gives

$$\left.\begin{aligned} \Delta T_d &= T_S - T_f = \frac{q/A}{h} - QN_{Pr}Y_B^+, && 0 \leqslant Y_B^+ \leqslant 5 \\ \Delta T_d &= \frac{q/A}{h} - 5Q\left\{N_{Pr} + \ln\left[1 + N_{Pr}\left(\frac{Y_B^+}{5} - 1\right)\right]\right\}, && 5 \leqslant Y_B^+ \leqslant 30 \\ \Delta T_d &= \frac{q/A}{h} - 5Q\left\{N_{Pr} + \ln\left[1 + 5N_{Pr}\right] + 0{\cdot}5\ln\left[\frac{Y_B^+}{30}\right]\right\}, && Y_B^+ \geqslant 30 \end{aligned}\right\} \tag{16}$$

* Equation (11) could have been employed in the subsequent sections. It should, however, require defining r_B in terms of Y_B, and thus would require knowledge of an additional arbitrary constant.

If the constants C and C' were known, equations (8) and (16) would determine the subcooled fluid conditions ΔT_d, i.e. the position, where vapor bubbles first leave the heated surface. To obtain the constants C and C', the equations were applied to some of the available experimental data. To simplify the calculations, all the liquid properties were taken at the saturation temperature, T_S. The heat-transfer coefficient was calculated from the accepted relation

$$\frac{hD_H}{k_L} = 0{\cdot}023\left(\frac{GD_H}{\mu_L}\right)^{0{\cdot}8}\left(N_{Pr}\right)^{0{\cdot}4}, \quad (17)$$

where k_L is the liquid thermal conductivity, and G is the mass flow rate per unit area. The wall shear stress τ_w is equal to

$$\tau_w = \frac{f}{8}\frac{1}{\rho_L}\frac{G^2}{g_c}, \quad (18)$$

where the friction factor, f, was obtained [7] from

$$f = 0{\cdot}0055\{1 + [20000(\epsilon/D_H) + 10^6/(GD_H/\mu_L)]^{\frac{1}{3}}\}. \quad (19)$$

The channel relative roughness parameter ϵ/D_H was taken to be that of drawn tubing, or $(\epsilon/D_H) = 10^{-4}$.

The above set of equations was applied first to high-velocity tests and the constant C was determined. The value of C' was next obtained from the low-velocity runs. It was found that for the range of reported test results

$$\left.\begin{aligned} C &= 0{\cdot}015 \\ C' &= 0. \end{aligned}\right\} \quad (20)$$

It is interesting to note that, according to equation (20), buoyant forces appear to play a negligible role even at the low mass flow rates of 100000 lb/h-ft^2 reported by Rouhani [8].

Once the constants C and C' are known, values of ΔT_d can be calculated for a multitude of test conditions; the predictions are listed in Tables 1–3. The values of ΔT_d for the high-pressure steam-water experiments of Bettis [2] and BMI [9] are given in Table 1. The measured values of ΔT_d reproduced in Table 1 are those reported by Bowring. The predicted and measured values of ΔT_d for Ferrell's [10] and

Table 1. Subcooling conditions for bubble departure for Bettis and BMI experiments

Experiments	Pressure (psia)	Mass flow rate (lb/h-ft^2)	Heat flux (Btu/h-ft^2)	Measured ΔT_d(°F)	Predicted ΔT_d(°F)
Bettis	1200	$0{\cdot}567 \times 10^6$	6×10^5	75	63
	1200	$0{\cdot}865 \times 10^6$	$6{\cdot}06 \times 10^5$	52	52
	1200	$0{\cdot}419 \times 10^6$	$1{\cdot}98 \times 10^5$	34	24
	1200	$0{\cdot}901 \times 10^6$	$6{\cdot}02 \times 10^5$	36	50
	1200	$0{\cdot}445 \times 10^6$	$0{\cdot}97 \times 10^5$	11	11
	1200	$0{\cdot}588 \times 10^6$	$3{\cdot}46 \times 10^5$	32	36
Bettis	1600	$0{\cdot}408 \times 10^6$	$0{\cdot}98 \times 10^5$	16	15
	1600	$0{\cdot}594 \times 10^6$	$1{\cdot}97 \times 10^5$	23	26
	1600	$0{\cdot}594 \times 10^6$	$2{\cdot}99 \times 10^5$	36	39
	1600	$0{\cdot}900 \times 10^6$	$2{\cdot}49 \times 10^5$	18	26
Bettis	2000	$0{\cdot}677 \times 10^6$	$3{\cdot}04 \times 10^5$	34	35
	2000	$0{\cdot}856 \times 10^6$	$3{\cdot}03 \times 10^5$	29	31
BMI	2000	$0{\cdot}673 \times 10^6$	$0{\cdot}8 \times 10^5$	8	9
	2000	$0{\cdot}405 \times 10^6$	$1{\cdot}5 \times 10^5$	17	23
	2000	$0{\cdot}662 \times 10^6$	$3{\cdot}0 \times 10^5$	23	35
	2000	$0{\cdot}654 \times 10^6$	$4{\cdot}0 \times 10^5$	32	48
	2000	$0{\cdot}840 \times 10^6$	$3{\cdot}0 \times 10^5$	25	31
	2000	$0{\cdot}844 \times 10^6$	$4{\cdot}0 \times 10^5$	38	41
	2000	$0{\cdot}844 \times 10^6$	$5{\cdot}0 \times 10^5$	31	52

Table 2. Subcooling conditions for bubble departure for Ferrell's experiments

Pressure (psia)	Mass flow rate (lb/h-ft^2)	Heat flux (Btu/h-ft^2)	Measured ΔT_d(°F)	Predicted ΔT_d(°F)
60	0.398×10^6	1.15×10^5	21	19
60	0.785×10^6	1.15×10^5	22	14
120	0.390×10^6	1.51×10^5	26	23
120	0.390×10^6	1.16×10^5	23	17
120	0.390×10^6	0.77×10^5	19	12
120	0.781×10^6	2.16×10^5	34	25
120	0.781×10^6	1.43×10^5	29	16
120	0.781×10^6	1.15×10^5	24	13
120	0.972×10^6	2.15×10^5	34	22
240	0.398×10^6	1.16×10^5	22	24
240	0.776×10^6	2.1×10^5	33	31

Table 3. Subcooling conditions for bubble departure for Rouhani's data

Pressure (psia)	Mass flow rate (lb/h-ft^2)	Heat flux (Bru/h-ft^2)	Measured ΔT_d(°F)	Predicted ΔT_d(°F)
142	0.0972×10^6	0.953×10^5	20	19
142	0.0973×10^6	1.87×10^5	34	38
142	0.781×10^6	1.87×10^5	28	21
142	0.781×10^6	2.82×10^5	37	32
142	1.061×10^6	1.87×10^5	21	19
142	0.391×10^6	2.96×10^5	38	45
425	0.0973×10^6	0.953×10^5	21	18
425	0.0973×10^6	1.87×10^5	40	35
425	0.0973×10^6	2.83×10^5	58	53
725	0.0973×10^6	1.87×10^5	32	37
725	0.0973×10^6	2.83×10^5	50	56

Rouhani's data are shown in Tables 2 and 3, respectively. Examination of Tables 1–3 reveal that the proposed model compares satisfactorily with the measurements. The calculated and the test values agree within ± 30 per cent. The agreement is all the more satisfactory when it is recognized that the low experimental vapor volumetric fractions found near the position of ΔT_d show considerable scatter, and that there are some inconsistencies in the test results. For instance, the last BMI run listed in Table 1 exhibits a different and probably incorrect trend with heat flux from that of the two runs preceding it.

The predicted effects of flow and fluid properties upon the departure subcooling ΔT_d are shown in Fig. 3. The values shown in Fig. 3 were calculated for steam–water mixtures and for a hydraulic diameter of 0·5 in and a heat flux of 250000 Btu/h-ft^2. Corresponding predictions obtained from Bowring's relations are plotted on the same figure. It is observed that the subcooling at bubble departure varies only slightly with pressure. The variation is of the same order of magnitude as that obtained from Bowring's equation. The present model, however, shows that the dependence upon pressure increases as the flow is reduced, and at low pressure, the prediction curves upward rather than staying horizontal. Both the proposed and Bowring's

equations predict that the subcooling ΔT_d decreases as the flow goes up. They are also in approximate agreement for mass flow rates of the order of $0{\cdot}5 \times 10^6$ lb/h-ft^2, where most of the available test data fall. The effects of flow rate, however, are reduced considerably in the present model. Higher subcooling values than Bowring's are predicted at high flows, and the inverse is true at low flows. The change of ΔT_d with flow becomes negligible at very low mass flow rates, and this accounts for the ability of the present model to predict Rouhani's data at $0{\cdot}1 \times 10^6$ lb/h-ft^2, a condition where Bowring's empirical correlation gives values substantially higher than measured.

The effects of heat flux and hydraulic diameter upon the subcooling ΔT_d are not included in Fig. 3. They can, however, be deducted from equation (16). According to equation (16), the subcooling ΔT_d is directly proportional to the heat flux, q/A, which agrees with Bowring's postulate. The hydraulic diameter also enters into equation (16) through the nondimensional distance Y_B^+ and the heat-transfer coefficient h. As the hydraulic diameter increases, so does Y_B^+ and the subcooling ΔT_d decreases at low values of Y_B^+. As Y_B^+ extends more and more into the turbulent core ($Y_B^+ > 30$), its effects upon ΔT_d become small and can be even reversed when the effects of the heat-transfer coefficient, h, start to predominate. It is interesting to note that while Bowring did not include a hydraulic diameter term, he reported that data taken at the Argonne National Laboratory [11] exhibited a dependence upon the hydraulic diameter. He found that the $\frac{1}{2}$-in ANL channel gave subcooling values smaller than the $\frac{1}{4}$-in channel. Bowring discarded the reported trend because he could not understand it physically. The explanation, now, can be inferred from equations (3 to 8). For the same flow velocity, the frictional pressure drop (i.e. the pressure differential exerted on the bubble in the flow direction) decreases as the hydraulic diameter is enlarged; the bubble must grow further into the main stream before it can detach itself from the wall and the resulting value of ΔT_d is reduced.*

As demonstrated in the case of hydraulic diameter, one of the important advantages of the present model is that it has a physical basis;

* Aemer Anderson (University of Illinois) has suggested to the author that the results of the analysis are represented best in terms of nondimensional groupings. Equation (9) can be rewritten as:

$$Y_B^+ = C\left(\frac{GD_H}{\mu_L}\right)\left(\frac{\sigma\rho_L g_c}{G^2 D_H}\right)^{-\frac{1}{4}} \tag{A-1}$$

Also, the subcooling at detachment can be normalized as follows:

$$\frac{T_w - T_s}{T_w - T_f} = 1 - \frac{T_s - T_f}{T_w - T_f} = 0{\cdot}023\left(\frac{GD_H}{\mu_L}\right)^{-0{\cdot}2} N_{Pr}^{-0{\cdot}6}\left(\frac{f}{8}\right)^{-0{\cdot}5} G(N_{Pr}, Y_B^+) \tag{A-2}$$

where

$$G(N_{Pr}, Y_B^+) = \begin{cases} N_{Pr}\, Y_B^+, & 0 < Y_B^+ < 5 \\ 5{\cdot}0\{N_{Pr} + \ln[1 + N_{Pr}(0{\cdot}2\, Y_B^+ - 1)]\}, & 5 < Y_B^+ < 30 \\ 5{\cdot}0\{N_{Pr} + \ln[1 + 5N_{Pr}] + 0{\cdot}5\ln(Y_B^+/30)\}, & Y_B^+ > 30 \end{cases}$$

The fractional subcooling

$$\frac{T_w - T_s}{T_w - T_f}$$

is a function of the dimensionless parameters

$$\frac{GD_H}{\mu_L}, \frac{G^2 D^H}{\sigma\rho_L g_c}, N_{Pr}, \text{and } f \quad \text{i.e.} \frac{GD_H}{\mu_L} \text{ and } \frac{\epsilon}{D_H}.$$

Typical values predicted by the model are shown in Figs. 4 and 5.

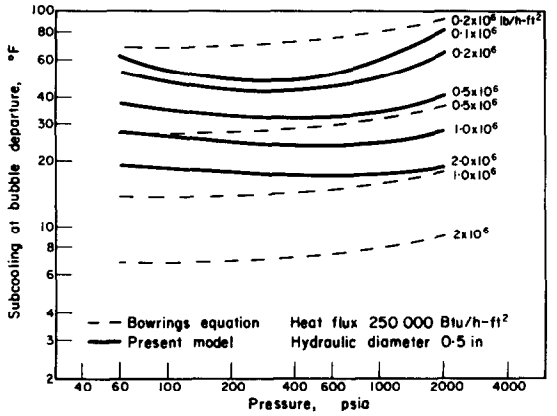

FIG. 3. Prediction of liquid subcooling at point of bubble departure for steam–water mixtures.

it can, therefore, be applied to flow conditions and fluids not previously tested. The following comments and words of caution are, however, in order before it is used indiscriminately.

1. At very low flow rates, the value of ΔT_d is obtained by subtracting two large numbers, and it becomes sensitive to the properties utilized. A more accurate treatment may be desirable for the heat-transfer coefficient and the temperature at which the properties are evaluated.
2. The constant C' in equation (7) was found to be zero for the range of available data. It can be expected that at extremely low flow rates, C' can no longer be neglected, and some data in this range may be desirable.

One more and final comment is in order about equation (6). Another relation was first tried for r_B, but it was found unsatisfactory and was discarded. In this initial approach, it was assumed that the force F_F was proportional to the wall shear stress and the surface of the bubble.

$$F_F = C_F \tau_w r_B^2. \tag{21}$$

so that

$$r_B = \frac{1}{2}\left\{-\frac{C_F \tau_w g_c}{C_B g(\rho_L - \rho_V)} + \left[\sqrt{\left(\frac{C_F \tau_w g_c}{C_B g(\rho_L - \rho_V)}\right)^2 + 4\frac{C_S \sigma g_c}{C_B g(\rho_L - \rho_V)}}\right]\right\}. \tag{22}$$

At very high flow rate, equation (22) reduces to

$$r_B = \frac{C_S \sigma}{C_F \tau_w}. \tag{23}$$

When compared to available test data, the above relation did not show the appropriate dependence upon flow, hydraulic diameter, and fluid

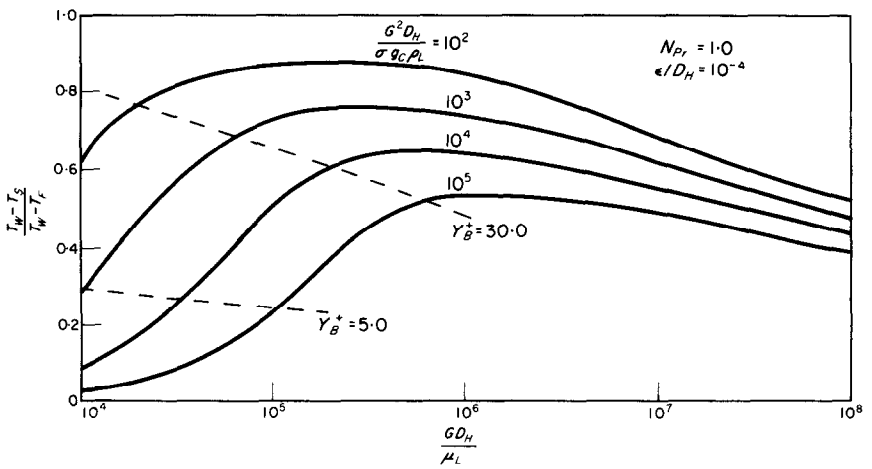

FIG. 4. Fractional wall superheat at bubble detachment for Prandtl number of one.

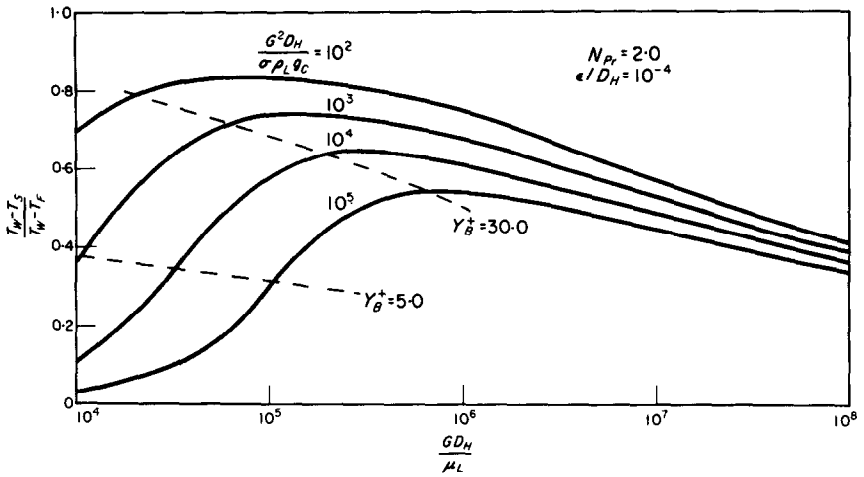

FIG. 5. Fractional wall superheat at bubble detachment for Prandtl number of two.

properties. The primary reason for mentioning equation (22) is that a similar form was proposed by Chang [12] in his studies of forced convection critical heat flux. Chang derived a similar expression for r_B by assuming that

$$F_F = C_F r_B^2 \rho_L \frac{U_{rel}^2}{g_c}, \tag{24}$$

where U_{rel} is the relative vapor velocity.* In view of the poor success of equation (22), some caution is in order in applying Chang's result.

3. VOLUMETRIC VAPOR FRACTION DURING SUBCOOLED FORCED CONVECTION

To calculate the local volumetric vapor fraction α in the subcooled region and beyond it, one must know the true local vapor weight fraction χ'. If χ is the local vapor weight fraction calculated from a heat balance and thermal equilibrium, χ' will have a finite value at positions where χ is zero and negative. As a matter of fact, we can postulate that at the point of bubble departure, χ' is approximately zero since at that location the bubbles are small and still attached to the heated surface. The corresponding value of χ at the same point is negative and equal to χ_d:

$$\chi_d = -\frac{C_{pL}\Delta T_d}{H_{fg}}. \tag{25}$$

Bubble motion is absent at the point of bubble departure, and most of the heat is being transferred to the liquid so that

$$\left.\frac{d\chi'}{dz}\right|_{z_d} = \left.\frac{d\chi'}{d\chi}\right|_{\chi_d} = 0. \tag{26}$$

As χ increases and becomes positive and large, nonthermal equilibrium conditions stop to exist and one can write that

$$\chi' \to \chi \text{ for } \chi \gg |\chi_d|. \tag{27}$$

A simple relation between χ' and χ which satisfies the above condition is

$$\chi' = \chi - \chi_d \exp\left(\frac{\chi}{\chi_d} - 1\right). \tag{28}$$

The basis and form of equation (28) is very similar to the one proposed by Zuber, Staub, and Bijwaard. The latter investigators postulated an exponential or hyperbolic tangent function for the local liquid subcooling in terms of the distance along the channel. Their expression is

* It is difficult to specify the relative velocity U_{rel} in the present case where the bubble is still attached to the wall.

more difficult to handle than equation (28) because to obtain the volumetric vapor fraction it requires integration with respect to position, and the integration becomes complicated for nonuniform heat flux distributions. The effects of variation in local heat flux were circumvented entirely in equation (28) by defining χ' in terms of the equilibrium weight fraction χ rather than the local position z.

Equation (28) specifies the value of χ' once the parameters χ and χ_d have been calculated from a heat balance and from the method proposed in the preceding section. The corresponding vapor volumetric fraction α is obtained by assuming that the relationship between α and χ' is the same as it would be under thermal equilibrium conditions. Several correlations are available in the literature for vapor volumetric fraction; and while, for example, one could have used the relations proposed in [13] and [14], the following equation proposed by Zuber and Findlay [15] was selected.

$$\alpha = \frac{\chi'}{\rho_V}\left\{1{\cdot}13\left[\frac{\chi'}{\rho_V}+\frac{1-\chi'}{\rho_L}\right] + \frac{1{\cdot}18}{G}\left[\frac{\sigma g g_c(\rho_L-\rho_V)}{\rho_L^2}\right]^{\frac{1}{4}}\right\}^{-1}. \quad (29)$$

In equation (29), the vapor volumetric distribution factor of 1·13 and the relative vapor bubbly drift velocity of 1·18

$$\left[\frac{\sigma g g_c(\rho_L-\rho_V)}{\rho_L^2}\right]^{\frac{1}{4}}$$

were taken as most typical of the range of test conditions covered in forced convection subcooled boiling tests. The validity of equation (29) is questionable. It has been shown in the literature that the vapor fraction distributions in developing flow differ from fully developed flow. In particular, the vapor distribution factor of 1·13 has been reported to be less than one. However, accurate developing flow correlations are not available; and the use of equation (29) is justified until such time that they are formulated.

Equations (28) and (29) were applied to a variety of experiments, and the results are plotted in Figs. 6–14. Figures 6 and 7 show experimental data obtained at Bettis in a rectangular channel, and the correspondence between tests and predictions is excellent. The model accurately predicts the vapor volumetric fraction over the entire range of vapor content. Similar satisfactory comparisons are noted in Fig. 8, where both Bettis and BMI data at 2000 psia are compared with the model. Figures 9 and 10 are plots of Christensen's data [16] at 400, 600, 800, and 1000 psia. While the agreement is excellent at the two high pressure values, some deviation between tests and predictions exists at 400 and 600 psia. The difference becomes noticeable beyond the subcooled region, and it appears that equation (29) is underestimating the local vapor slip. Some of Ferrell's data are shown in Figs. 11 and 12. In this case,

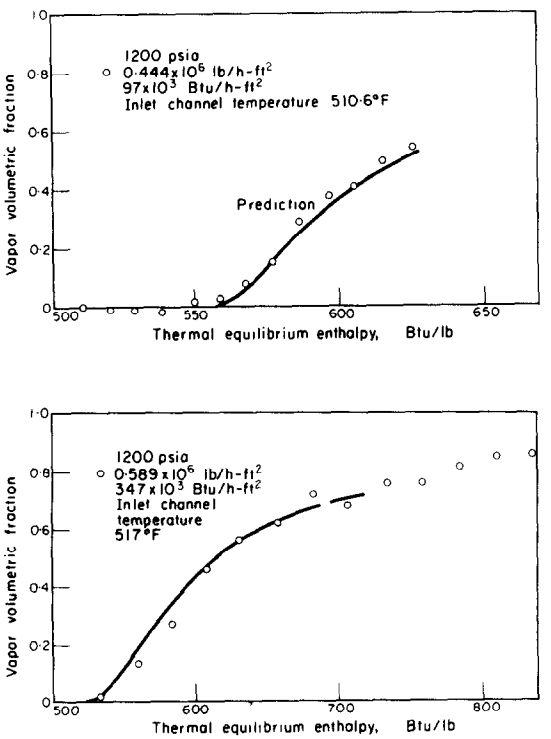

FIG. 6. Comparison of model with Bettis data at 1200 psia.

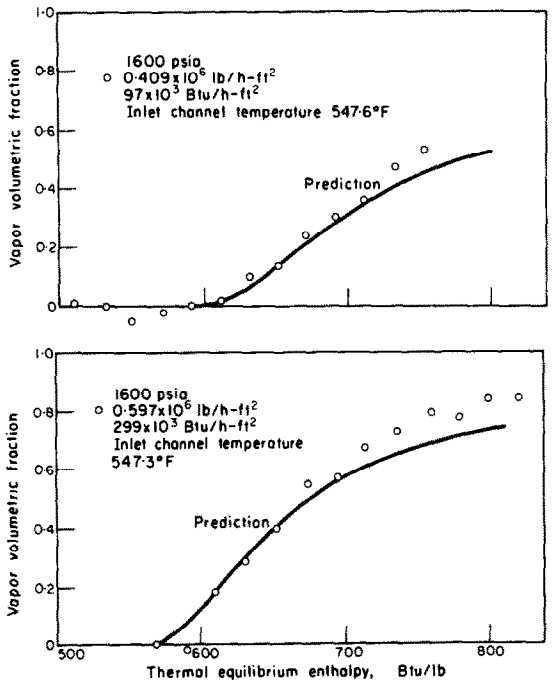

FIG. 7. Comparison of model with Bettis data at 1600 psia.

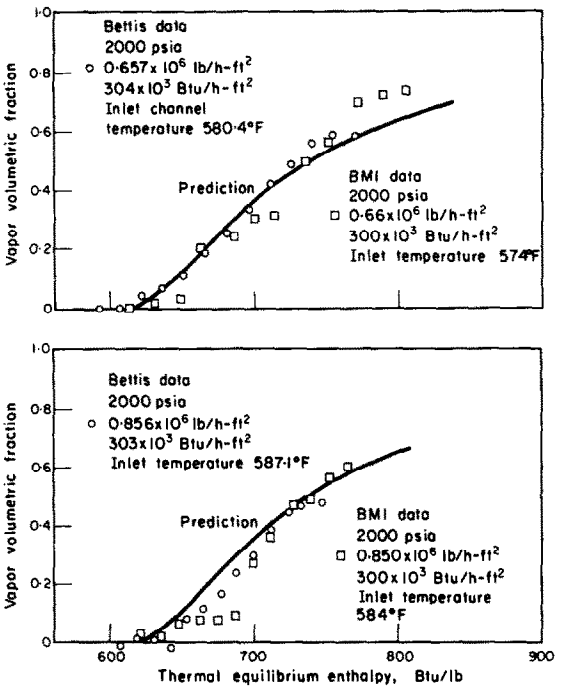

FIG. 8. Comparison of model with Bettis and BMI data at 2000 psia.

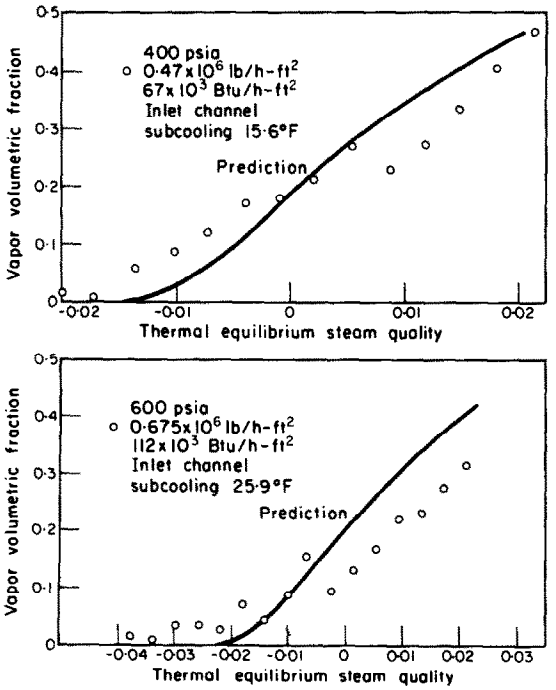

FIG. 9. Comparison of model with Christensen's data at 400 and 600 psia.

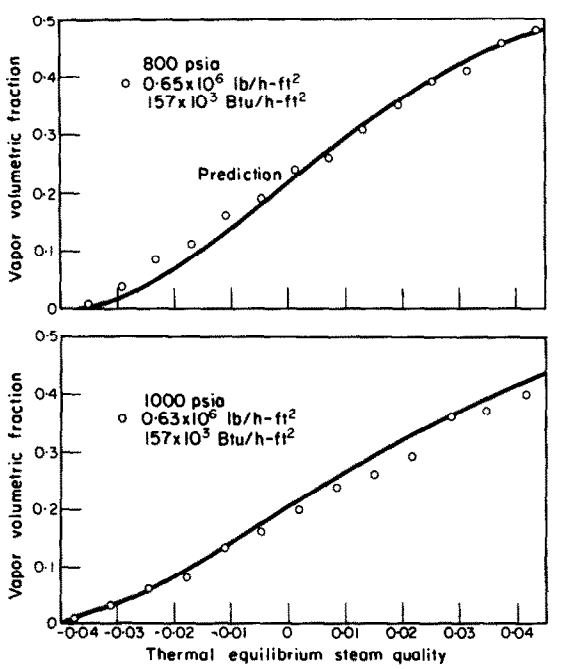

FIG. 10. Comparison of model with Christensen's data at 800 and 1000 psia.

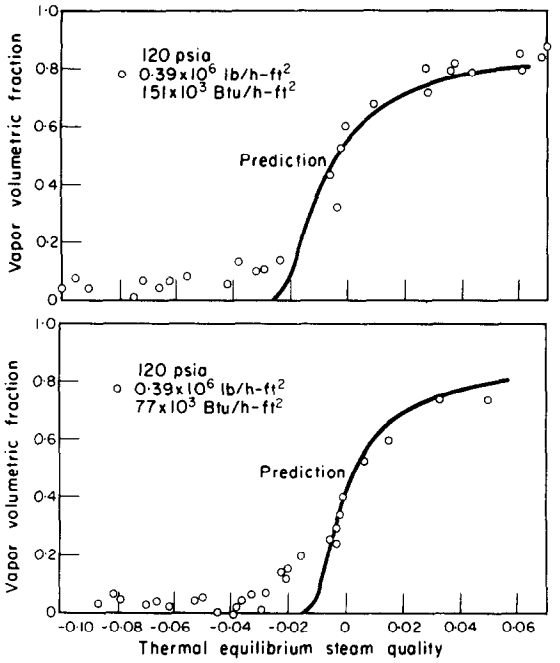

FIG. 11. Comparison of model with Ferrell's data at 120 psia.

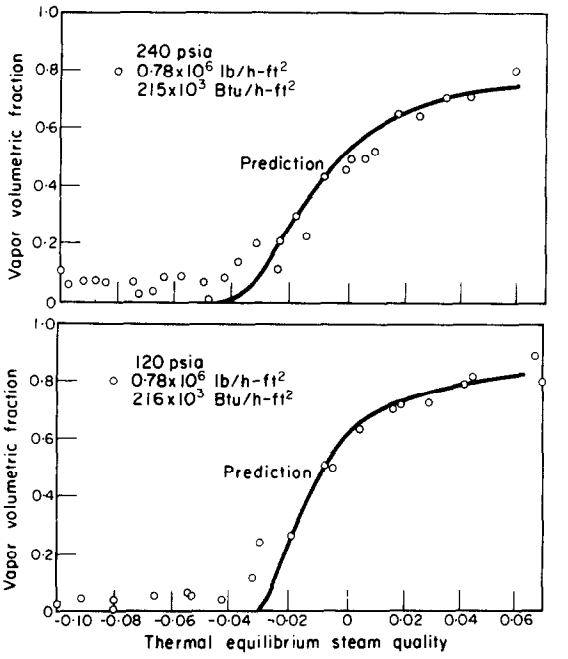

FIG. 12. Comparison of model with Ferrell's data at 120 and 250 psia.

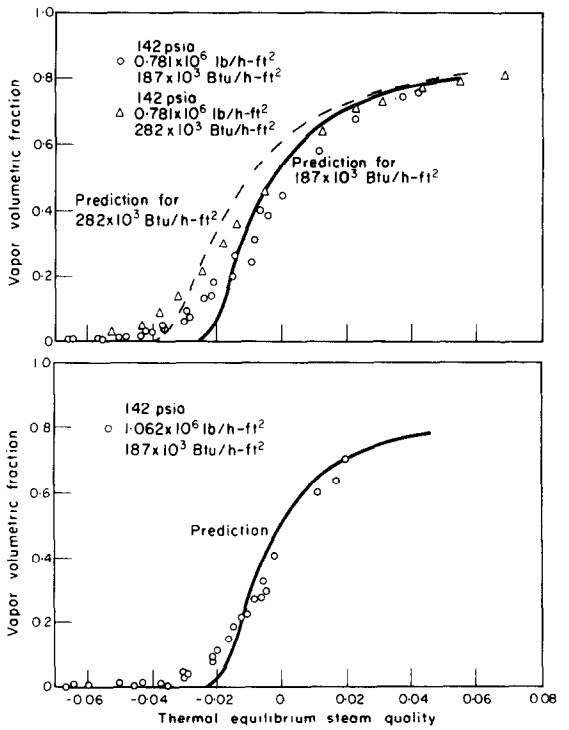

FIG. 13. Comparison of model with Rouhani's data at high flow rates.

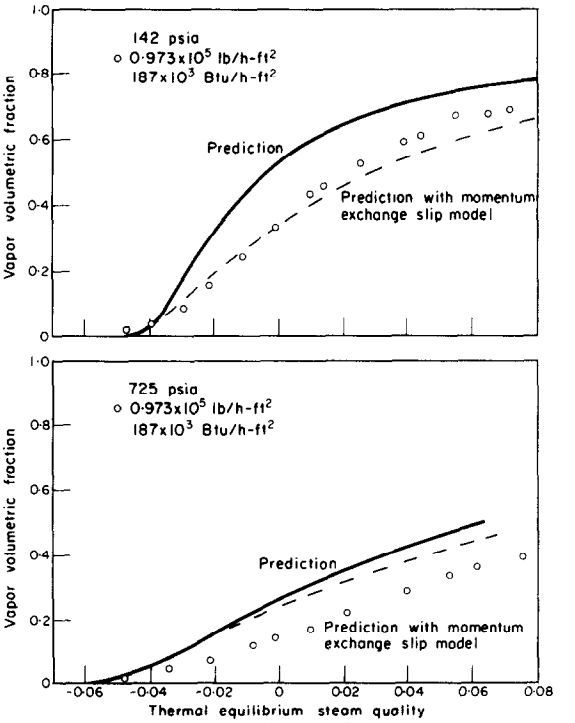

FIG. 14. Comparison of model with Rouhani's data at low flow rates.

the agreement beyond the subcooled region is very good, and the initial vapor volumetric fractions look low. This can be traced to the tendency to underpredict ΔT_d for Ferrell's runs. Yet, the model predictions at zero steam quality fall on top of the data, and the agreement at this location would be adversely affected if the predicted subcoolings ΔT_d were to be increased. Shown in Fig. 13 are Rouhani's data at medium and high velocity, and here again, the model is doing a satisfactory job. At the very low flow rates considered in Fig. 14, the model tends to overpredict the vapor volumetric fraction. The deviation is due to the fact that equation (29) gives too low a vapor slip velocity value. It is also possible that at low mass flow rates, the acceleration losses become dominant; for this reason, the momentum exchange model of [17] which considers mostly acceleration losses was substituted for equation (29). The agreement improved considerably at all pressures except at 725 psia where, as shown in Fig. 14, even the momentum model overpredicted the vapor volumetric fraction. It appears, therefore, that at low flows the local vapor slip values in Rouhani's tests do not follow expected trends and the increased slip values he obtained may be brought about by the fact that his tests were performed in an internally heated annulus.

The predicted effects of heat flux, pressure, and flow rate upon the subcooled vapor volumetric fraction can be deduced from Figs. 6–14. Figure 13 shows that the subcooled volumetric fraction, α, increases as the heat flux goes up. Similarly, as it would be expected, the subcooled values of α increase as the pressure is reduced (Fig. 12). Decreasing the flow rate has generally the same effect as can be seen from Fig. 13. Moreover, at very low flow rate, the local vapor drift velocity can negate and even reverse this trend. Finally, the role of hydraulic diameter can be inferred from the proposed equations. As the diameter increases, the subcooling ΔT_d decreases, and so will the subcooled volumetric vapor friction.

It is also interesting to note that equation (28) can be used to specify the fraction of heat q_v going to form vapor.

$$q_v = A_F G H_{fg} \frac{d\chi'}{dz}, \tag{30}$$

where A_F is the flow area.

Substitution of equation (28) and recognizing that

$$q = A_F G H_{fg} \frac{d\chi}{dz} \tag{31}$$

gives

$$\frac{q_v}{q} = 1 - \left(\exp \frac{\chi}{\chi_d} - 1\right). \tag{32}$$

According to equation (32), the ratio q_v/q changes with position and is not a constant as predicted by Bowring.

In the preceding derivations, it was assumed that the vapor volumetric fraction was equal to zero at the point of bubble departure. A high estimate of the vapor present at that location can be obtained as follows. Let us assume that the vapor bubbles are spaced a distance S apart. The number of bubbles around the wetted perimeter P_W is then (P_W/S). If the bubbles are assumed to be full spheres (i.e., $Y_B = 2r_B$), their volume in a section of channel S long is (P_W/S) $(\frac{4}{3}\pi r_B^3)$; the volumetric fraction of vapor α_d at that position is

$$\alpha_d = \left(\frac{P_W}{S}\right)\left(\tfrac{4}{3}\pi r_B^2\right)\frac{1}{A_F S} = \frac{16\pi}{3}\frac{r_B}{D_H}\left(\frac{r_B}{S}\right)^2. \tag{33}$$

If the bubbles are assumed to be packed in a square array and to interfere with each other area of influence, $r_B/S \approx 0{\cdot}25$ and

$$\alpha_d \approx \frac{\pi}{3}\frac{r_B}{D_H} \approx \frac{\pi}{6}\frac{Y_B}{D_H}. \tag{34}$$

Typical values of α_d calculated from equation (34) for steam-water mixtures flowing at various

pressures in a channel of hydraulic diameter of 0·5 in and at a heat flux of 250,000 Btu/h-ft^2 are tabulated below.

Table 4

Pressure (psia)	Flow rate		
	0·1 × 10^6 lb/h-ft^2	0·5 × 10^6 lb/h-ft^2	1 × 10^6 lb/h-ft^2
60	$\alpha_d = 5{\cdot}5 \times 10^{-2}$	$\alpha_d = 1{\cdot}3 \times 10^{-2}$	$\alpha_d = 0{\cdot}7 \times 10^{-2}$
300	$\alpha_d = 4{\cdot}7 \times 10^{-2}$	$\alpha_d = 1{\cdot}1 \times 10^{-2}$	$\alpha_d = 0{\cdot}6 \times 10^{-2}$
600	$\alpha_d = 4{\cdot}0 \times 10^{-2}$	$\alpha_d = 1{\cdot}0 \times 10^{-2}$	$\alpha_d = 0{\cdot}5 \times 10^{-2}$
1000	$\alpha_d = 3{\cdot}3 \times 10^{-2}$	$\alpha_d = 0{\cdot}8 \times 10^{-2}$	$\alpha_d = 0{\cdot}4 \times 10^{-2}$
2000	$\alpha_d = 1{\cdot}9 \times 10^{-2}$	$\alpha_d = 0{\cdot}5 \times 10^{-2}$	$\alpha_d = 0{\cdot}2 \times 10^{-2}$

The volumetric fractions α_d are observed to decrease with increased pressures and flow rates. Also, except for the low flow condition, the values of α_d are small. It is interesting to compare the values of bubble diameter at departure from the present model with the observations of Hosler [18]. Hosler reported that bubbles detach from the wall while quite small (at most of the order of 0·003–0·005 in. in diameter). The present model predicts that the bubble diameter at detachment will be of the order of 0·003 in for the test conditions of Hosler and a flow rate of 0·5 × 10^6 lb/h-ft^2, and the agreement is surprisingly good.

4. CONCLUSIONS

1. A method was developed to predict vapor volumetric fractions during subcooled forced convection boiling.
2. The method gives general agreement with the available data.

ACKNOWLEDGEMENT

The author is especially indebted to J. M. Healzer who set up all of the model calculations on the computer and carried out most of the computations.

REFERENCES

1. R. W. Bowring, Physical model, based on bubble detachment, and calculation of steam voidage in the subcooled region of a heated channel, HPR-29, Institutt for Atomenergi, Halden, Norway.
2. P. Griffith, J. A. Clark and W. M. Rohsenow, Void volumes in subcooled boiling systems, ASME Paper No. 58-HT-19 (1958).
3. G. W. Maurer, A method of predicting steady-state boiling vapor fractions in reactor coolant channels, Bettis Technical Review, pp. 59–70 (1960).
4. N. Zuber, F. W. Staub and G. Bijwaard, Vapor void fractions in subcooled boiling and in saturated boiling systems, Third International Heat Transfer Conference, Chicago, Illinois (August 1966).
5. Y. Y. Hsu, On the size range of active nucleation cavities on a heating surface, *J. Heat Transfer* **84C**, 207 (1962).
6. R. C. Martinelli, Heat transfer to molten metals, *Trans. Am. Soc. Mech. Engrs* **69**, 947 (1947).
7. J. P. Waggener, Friction factors for pressure drop calculations, *Nucleonics* **19**, 145 (1961).
8. S. Z. Rouhani, Void measurements in the region of sub-cooled and low-quality boiling, Symposium on Two-Phase Flow, University of Exeter (June 1965).
9. R. A. Egen, D. A. Dingee and J. W. Chastain, Vapor formation and behavior in boiling heat transfer, BMI 1163 (1957).
10. J. K. Ferrell, A study of convection boiling inside channels, North Carolina State University, Raleigh, North Carolina (September 1964).
11. J. F. Marchaterre, M. Petrick, P. A. Lottes, R. J. Weatherhead and W. S. Flinn, Natural and forced circulation boiling studies, ANL-5735 (1960).
12. Y. P. Chang, An analysis of the critical conditions and burnout in boiling heat transfer, USAEC Report TID-14004 (1961).
13. P. Griffith, The prediction of low-quality boiling void, ASME Paper No. 63-HT-20 (1963).
14. J. F. Marchaterre and B. M. Hoglund, Correlation for two-phase flow, *Nucleonics* **20** (8), 142 (1962).
15. N. Zuber and J. Findlay, Average volumetric concentration in two-phase flow systems, *J. Heat Transfer* **87C**, 453 (1965).
16. H. Christensen, Power-to-void transfer functions, ANL-6385 (1961).
17. S. Levy, Steam slip-theoretical predictions from momentum model, *J. Heat Transfer* **82C**, 113 (1960).
18. E. R. Hosler, Visual study of boiling at high pressure, CEP Symposium Series No. 57, *Heat Transfer*, Vol. 61, pp. 269–279. Boston (1965).

Résumé—Un modèle destiné à prédire la fraction volumique de vapeur pendant l'ébullition sous-refroidie par convection forcée est exposé. La méthode de calcul proposée consiste en trois étapes:

1. Le point de départ des bulles de la surface chauffée (c'est-à-dire, l'emplacement où les fractions volumiques de vapeur sont sensiblement plus élevées que zéro) est déterminé à partir d'un bilan de forces sur les bulles et de la distribution de température loin de la surface chauffée dans une phase liquide unique turbulente.
2. On suppose qu'il existe une certaine relation entre la véritable fraction massique de vapeur locale et la valeur correspondant à l'équilibre thermique.
3. On obtient la fraction volumique de vapeur à partir de la véritable fraction massique de vapeur locale et d'une relation connue entre les fractions massiques et volumique de vapeur.

La méthode a été appliquée à un ensemble de données expérimentales disponibles, et l'accord était satisfaisant pour un grand nombre de conditions d'écoulement, de flux de chaleur et de propriétés de fluides.

Zusammenfassung—Zur Bestimmung des volumetrischen Dampfanteils bei unterkühltem Sieden in freier Konvektion wurde ein Modell entwickelt. Die vorgeschlagene Berechnungsmethode besteht aus 3 Schritten:

1. Die Stelle der Blasenablösung von der beheizten Wand (d.h. der Ort mit einem volumetrischen Dampfanteil wesentlich grösser als null) wird bestimmt aus einer Bilanz der Blasenkräfte und der turbulenten Temperaturverteilung in der Flüssigkeit im Abstand von der beheizten Wand.
2. Eine Beziehung wird aufgestellt zwischen dem wahren örtlichen Dampfgewichtsanteil und dem entsprechenden Wert des thermischen Gleichgewichts.
3. Der volumetrische Dampfanteil wird erhalten aus dem wahren örtlichen Dampfgewichtsanteil und einer anerkannten Beziehung zwischen Dampfgewicht und volumetrischem Anteil.

Die Methode wurde auf eine Reihe von Versuchsdaten angewandt, und es zeigt sich zufriedenstellende Übereinstimmung für eine Vielzahl von Strömungen, Wärmestromdichten und Flüssigkeitseigenschaften.

Аннотация—Разработана модель для расчета истинного объемного парасодержания при кипении недогретой жидкости в условиях вынужденной конвекции. Предложенный метод расчета состоит из трех операций:

1. По балансу силы пузырька и распределению температуры однофазной турбулентной жидкости на некотором расстоянии от нагретой стенки определяется точка отрыва пузырька от поверхности нагрева (т.е. место, где объемное парасодержание значительно выше нуля).
2. Постулируется соотношение между истинным локальным весовым парасодержанием и соотвествующей величиной при тепловом равновесии.
3. Объемное парасодержание получается из истинного весового парасодержания; принимается соотношение между весовым и объемным парасодержанием.

Этот метод применяется для ряда экспериментальных данных. Получено удовлетворительное согласование для различных режимов течения, тепловых нагрузок и свойств жидкостей.